Ultra-wideband Inkjet Printed Grounded Coplanar Waveguide-to-Folded Waveguide Transition

Berkay Dogan, Dimitra Psychogiou
Tyndall National Institute, Cork, Ireland
University College Cork, School of Engineering, Cork, Ireland
berkay.dogan@tyndall.ie, Dpsychogiou.ucc.ie

***Abstract*—This paper presents the design and practical development of an ultra-wideband 3D grounded coplanar waveguide (GCPW)-to-folded waveguide (FWG) transition for beamforming antenna systems in X/Ku-band. It is based on a two-stage configuration comprising a three-dimensional (3D) vertical taper transition and a shielded stripline. A novel integration concept using a two-material piezo drop-on-demand process is proposed for ultra-compact 3D monolithic integration. For proof-of-concept validation purposes, a prototype comprising two transitions in a back-to-back configuration was designed and tested. It exhibited a center frequency of 13.3 GHz, a 10-dB return loss (RL) bandwidth (BW) from 9.08 GHz to 17.54 GHz, (i.e., absolute BW of 8.46 GHz) and a fractional BW (FBW) of 63.61 %. In this BW, the in-band insertion loss (IL) was measured between 1.05-3.66 dB.**

***Index Terms*—Additive manufacturing (AM), inkjet printing, monolithic integration, 3D printing, transition, waveguide theory.**

I. Introduction

The rapid growth of wireless communication networks is increasingly calling for broadband antenna systems able to support a wide variety of applications within the same RF transceiver [1], [2]. At higher frequencies or for applications requiring high power handling, waveguide (WG)-based integration schemes are typically preferred for the realization of high performing antenna systems. However, their operation relies heavily on the availability of high performing transitions to allow their interconnection with standardized coaxial interfaces [3]. Alternative transition types have been presented for WG components. For instance, microstrip-to-WG transitions were demonstrated in [4] and [5]. However, they are bulky and rely on multi-split-block integration, and their fractional bandwidth (FBW) is limited to 12%. To increase the operating BW, grounded coplanar waveguide (GCPW)-to-WG transition concepts have been introduced in [6]-[9] based on an antenna structure that excites the dominant mode of a rectangular WG. However, their FBW is also limited to 47.6%.

Transitions for folded waveguide (FWG)-based microwave systems have also been proposed due the small footprint of FWGs which is at least 50% smaller than conventional WGs. However, the realization of FWG components relies on complex multilayer PCB-based or multi-part assemblies that require post-fabrication tuning. Furthermore, most of the reported microstrip or GCPW-to-FWG transitions have a limited FBW [10]-[13].

Recent advancements in additive manufacturing technologies are paving the way to high performing 3D RF components and antenna systems with complex/intricate 3D structural geometries due to their freeform manufacturing capabilities [14], [15]. Recently a very promising Light-Out Digital Manufacturing (LDM) piezo drop-on-demand two-material process [16] was introduced for the manufacturing of self-packaged and monolithic RF components including antennas, bandpass filtering baluns [17], [18] and FWG-based bandpass filters [19]. However, they have not yet been used for the realization of 3D WG transitions.

This paper reports on a new type of an ultra-wideband 3D GCPW-to-FWG transition alongside a detailed design methodology. The proposed design concept is based on a

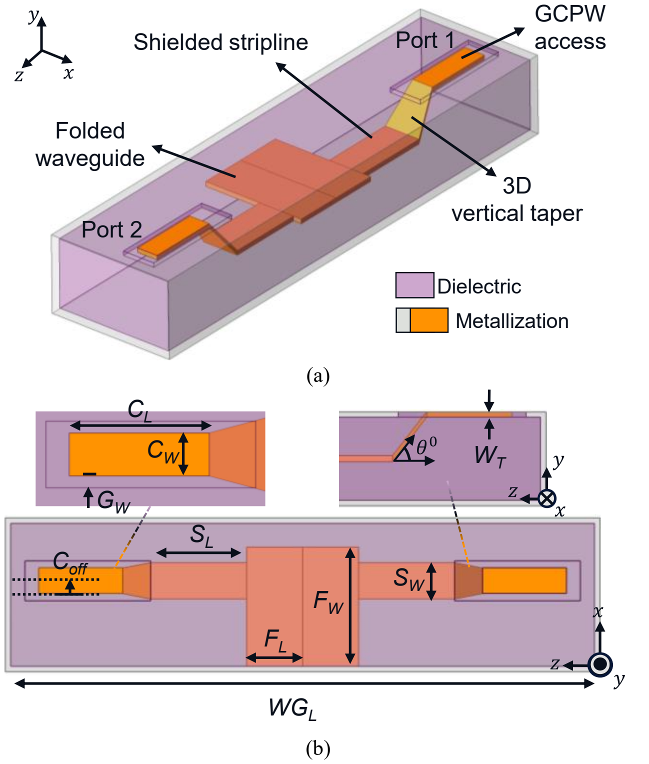

Fig. 1. (a) 3D geometry (bird's-eye view) and EM simulation model of the GCPW-to-FWG transition. (b) Top view of the GCPW-to-FWG transition, showing the GCPW details along with transition angle in the inset. In this example, dimensions are as follows: C_W = 0.918 mm, G_W = 0.252 mm, C_L = 3 mm, W_T = 0.183 mm, C_{off} = 0.775 mm, S_L = 3.22 mm, S_W = 1.58 mm, F_L = 2 mm, F_W = 4.475 mm, $\theta^0 = 52.87^0$, WG_L = 20.84 mm.

two-stage configuration comprising a 3D vertical taper transition and a shielded stripline, whose characteristics are determined using full-wave electromagnetic (EM) analysis in ANSYS HFSS. A novel integration approach aimed at monolithic integration and size compactness is employed using an in-house two-material LDM printer. For proof-of-concept validation purposes, an experimental prototype comprising two transitions in a back-to-back configuration was designed, manufactured and tested.

II. THEORETICAL FOUNDATIONS

A. *FWG and Shielded Stripline Designs*

The 3D model of the proposed GCPW-to-FWG transition is shown in Fig. 1. The ultra-wideband transition is performed in two stages, namely a 3D vertical taper transition and a shielded stripline that smoothly convert the electric (E) of the GCPW to the E-field of the FWG while matching the waveguide impedances at each stage. The proposed design is enabled by the free-form manufacturing capabilities of a two-material piezo drop-on-demand LDM platform that supports an acrylate dielectric ink (DI) that has a relative permittivity (ε_r) of 2.8 and loss tangent of 0.02, and a conductive ink (CI) with a conductivity (σ) of 1.8x10^6 S/m.

The design starts by analyzing the characteristics of the 3D FWG. Its geometry and the E-field distribution of the fundamental mode are shown in Fig. 2(a). In Fig. 2(b), the mode propagation characteristics are provided in terms of phase constant (β) and wave impedance (Z_W) of the fundamental mode. They have been obtained with full-EM simulations in the software package ANSYS. As it can be seen, by altering the width of the septum (F_W) while keeping the rest of the geometrical parameters constant [i.e., the waveguide width (WG_W), the waveguide height (WG_H), and the folded septum thickness (F_T)], the first mode shifts to lower frequencies, while the second mode remains stable allowing to widen the monomode BW. The Z_W of the first mode is also evaluated for different F_W values while keeping the other parameters constant. As it can be seen, increasing F_W results in a lower Z_W. The detailed performance parameters, including the first two cutoff frequencies (f_{c1} and f_{c2}), the monomode BW, and the Z_W computed at 13 GHz are provided in Table. I. Considering a target Z_W of 50 Ω at 13 GHz, the F_W is set to 4.25 mm, resulting in a monomode operating BW of 8.43 GHz (8.51- 16.93 GHz). The final FWG dimensions are as follows: WG_W = 5.1 mm, WG_H = 2.9 mm, F_T = 0.2 mm, and F_W = 4.25 mm.

TABLE I. BW AND Z_W OF THE FWG AS A FUNCTION OF F_W

F_W (mm)	f_{c1} (GHz)	f_{c2} (GHz)	BW (GHz)	Z_W (Ω) at 13 GHz
4.1	8.87	16.92	8.05	53.07
4.2	8.63	16.93	8.30	50.76
4.3	8.40	16.94	8.54	47.79
4.4	8.15	16.96	8.81	45.51
4.5	7.88	16.97	9.09	43.21

Having designed the FWG, the characteristics of the shielded stripline section are specified next through full-wave EM simulations in the software package ANSYS HFSS and are summarized in Fig. 3 in terms of its geometrical details [see Fig. 3(a)], BW and impedance characteristics [see Fig. 3(b)]. As can it be seen, altering the strip width (S_W) while keeping the strip thickness (S_T) equal to F_T, does not affect the monomode BW. On the other hand, if S_W increases, the Z_W of the first mode shifts to lower values due to the increased capacitance between the strip ends and the outer walls.

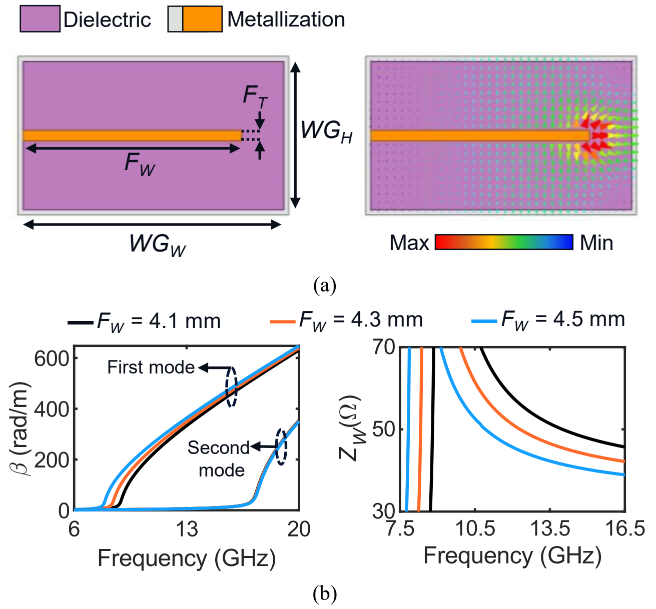

Fig. 2. Front view of the FWG. (a) Geometrical details (left). E-field distribution of the fundamental mode (right). (b) Phase constant (β) of the first two modes (left), and Z_W (right) as a function of F_W .

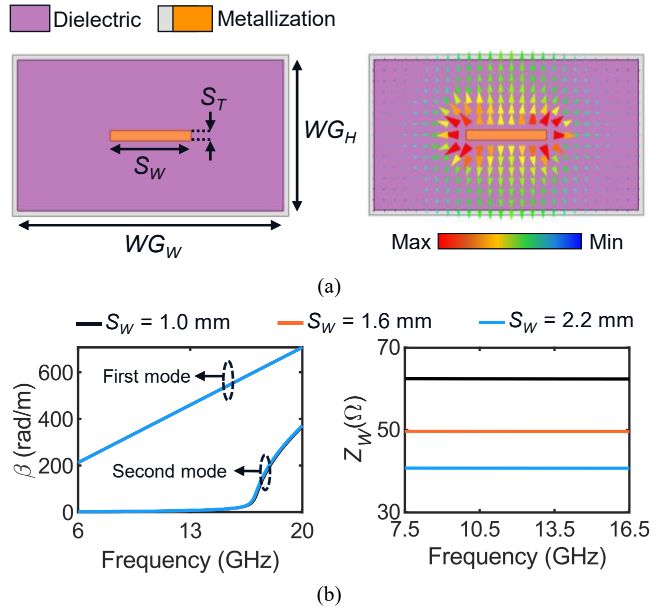

Fig. 3. Front view of the stripline. (a) Geometrical details (left). E-field distribution of the fundamental mode (right). (b) Phase constant (β) of the first two modes (left), and Z_W (right) as a function of S_W.

Considering a target input Z_W of 50 Ω at 13 GHz, S_W is set to 1.55 mm, resulting in a monomode BW of 16.58 GHz.

B. GCPW-to-FWG Transition

The GCPW accesses have been optimized for a 50 Ω impedance considering RF testing using 800-µm GSG probe tips. Subsequently, a 3D vertical taper transition is incorporated to facilitate connectivity between the GCPW and the stripline exploiting the 3D design freedom offered by the two-material inkjet process, as shown in Fig. 4(a). The EM-simulated S-parameters of the GCPW to the shielded stripline transition are provided in Fig. 4(b) using the geometrical dimensions in the caption of Fig. 4. They demonstrate a 10 dB operational BW up to 19.66 GHz, with an IL less than 1.25 dB.

Having designed each stage of the transition, they are then combined together in a single geometry as shown in Fig. 5. Additionally, an offset (C_{off}) is introduced to mitigate the reflections caused by the discontinuity between the FWG and the shielded stripline. The S-parameter response of the GCPW-to-FWG transition is provided in Fig. 5(b), exhibiting a 10-dB RL BW of 8.11 GHz (9.08–17.2 GHz) with a minimum in-band IL of 0.65 dB. Furthermore, the EM-simulated RF performance of the transition is evaluated in a back-to-back configuration and is shown in Fig. 6(b), demonstrating a 10-dB RL BW of 7.72 GHz (9.48–17.2 GHz) with a minimum in-band IL of 1.18 dB. The final dimensions are given in the caption of Fig. 1.

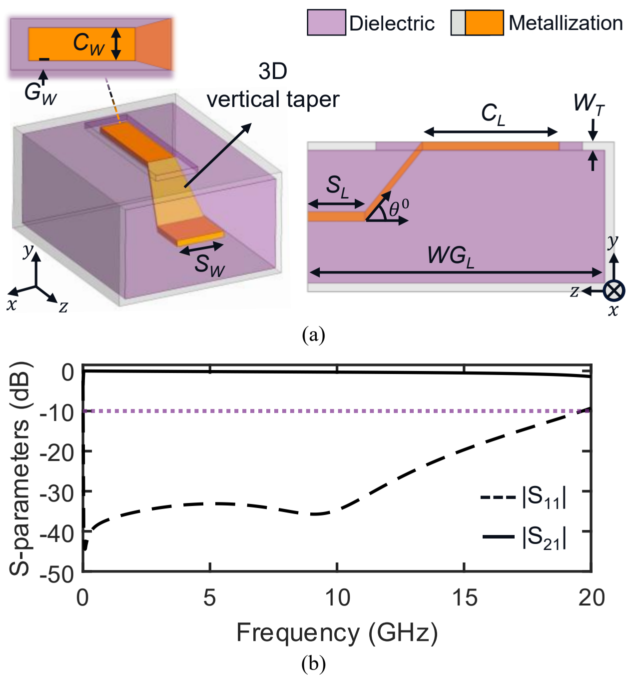

Fig. 4. 3D EM simulation model of the GCPW-to-shielded stripline transition. (a) Bird's-eye view (left) and side view (right). The geometrical details of GCPW access are shown in the inset. (b) EM-simulated S-parameters. In this example, dimensions are as follows: C_W = 0.918 mm, G_W = 0.252 mm, S_W = 1.58 mm, S_L = 1.25 mm, θ^0 = 51.73^0, C_L = 3 mm, W_T = 0.183 mm, WG_L = 6.5 mm.

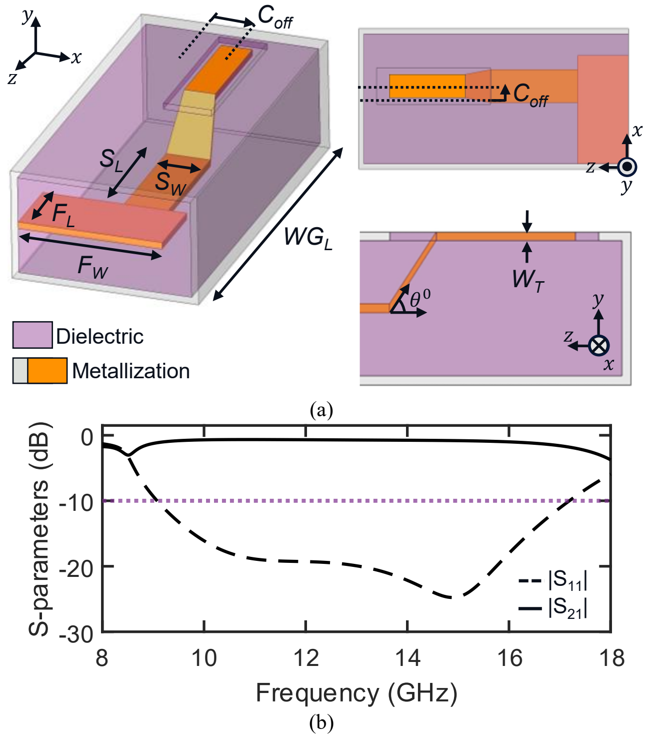

Fig. 5. 3D EM simulation model of the GCPW-to-FWG transition. (a) Bird's-eye view (left), top view (right-top), side view (right-bottom). (b) EM-simulated S-parameters. In this example, dimensions are as follows: W_T = 0.183 mm, C_{off} = 0.5 mm, S_L = 3.42 mm, S_W = 1.3 mm, F_L = 2 mm, F_W = 4.25 mm, θ^0 = 57.35^0, WG_L = 10.42 mm.

III. Experimental Validation

To validate the proposed GCPW-to-FWG transition concept, a prototype with two transitions in a back-to-back configuration was designed, manufactured, and tested. For structural integrity, a 0.325 mm-thick dielectric wall was added around the metallic walls, as shown in Fig. 6(a). Additionally, the GCPW is filled with dielectric ink to enhance structural integrity. Manufacturing was carried out using a piezo-drop on demand inkjet printer that features two independent printheads (i.e., one for the CI and another for the DI ink) facilitating simultaneous layer-by-layer deposition. Finally, the manufactured prototype of the transition is illustrated in Fig. 6(a). The inset in Fig. 6(b) illustrates the printing orientation. The surface roughness of the metallized waveguide walls was measured around 1.26 μm (Ra).

RF testing was performed using a Keysight PNA-X N5247B network analyzer and 800 µm GSG RF probes. Its RF measured performance is provided in Fig. 6(b). It exhibits a center frequency of 13.3 GHz, a 10 dB-BW of 8.46 GHz (from 9.08 GHz to 17.54 GHz, and an FBW of 63.61%. In this BW, the IL was measured between 1.05-3.66 dB. Furthermore, the manufactured prototype has a volume of 0.025 λ_0^3 and only weighs 0.78 g.

A comparison of the proposed transition with state-of-the-art GCPW-to-FWG transitions is provided in Table II. To the

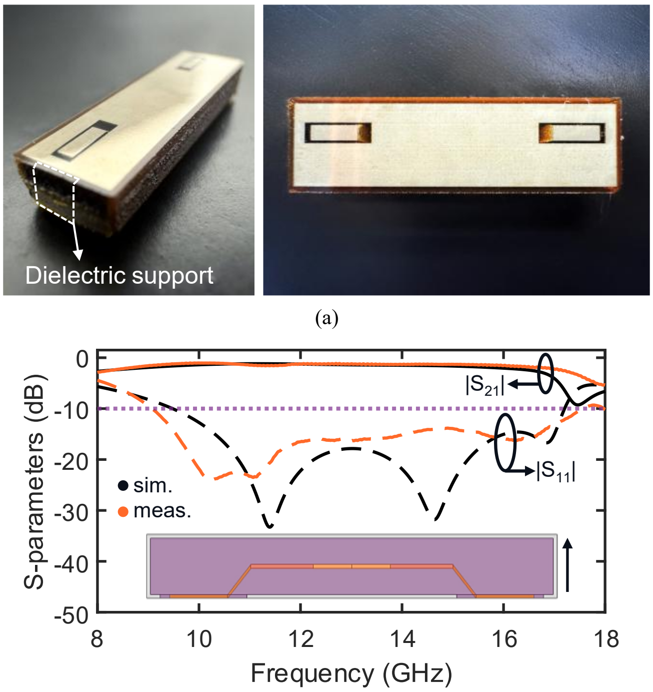

(b)

Fig. 6. Experimental validation of the GCPW-to-FWG transition. (a) Photograph of the manufactured prototype. Bird's-eye view (left). Top view (right). (b) EM-simulated and RF-measured S-parameters. The inset demonstrates the printing orientation.

best of the authors' knowledge, this work represents the first monolithically integrated 3D transition that exhibits an ultra-compact size of only 0.025 λ_0^3, which is up to more than 5 times smaller than the PCB-based counterparts reported in [10], and [11]. Lastly, as a significant advantage to be highlighted the proposed GCPW-to-FWG transition exhibits the widest reported FBW, surpassing all the transition concepts reported in the literature.

IV. Conclusion

In this paper, the design and practical development of an ultra-wideband 3D GCPW-to-FWG transition for beamforming antenna systems in X/Ku-band is reported. It consists of a two-stage configuration using a 3D vertical taper transition and a shielded stripline. To enable ultra-compact 3D monolithic integration, a novel manufacturing method using a two-material piezo drop-on-demand process is proposed. For proof-of-concept validation purposes, a prototype comprising two transitions in a back-to-back configuration was designed and tested. It shows RF performance as follows: a center frequency of 13.3 GHz, a 10-dB return loss BW from 9.08 GHz to 17.54 GHz, (i.e., absolute BW of 8.46 GHz) and an FBW of 63.61%. Within this BW, the measured in-band IL ranged from 1.05 dB to 3.66 dB. The manufactured prototype has a volume of 0.025 λ_0^3 and only weighs 0.78 g.

Acknowledgment

This work was supported by Research Ireland, Grant numbers: 13/RC/2077_P2 and 20/RP/8334.

References

[1] S. Zhang, J. Liu, H. Guo, M. Qi and N. Kato, "Envisioning device-to-device communications in 6G," in *IEEE Network*, vol. 34, no. 3, pp. 86-91, May/June 2020.

[2] H. Tataria, M. Shafi, A. F. Molisch, M. Dohler, H. Sjöland and F. Tufvesson, "6G wireless systems: vision, requirements, challenges, insights, and opportunities," in *Proceedings of the IEEE*, vol. 109, no. 7, pp. 1166-1199, July 2021.

[3] A. Fontana, A. Delage, A. Perigaud, P. Richard, D. Carsenat, G. Acikalin, S. Verdeyme, B. Bonnet, L. Carpentier, and N. Delhote., "A novel approach toward the integration of fully 3-D printed surface-mounted microwave ceramic filters," in *IEEE Transactions on Microwave Theory and Techniques*, vol. 71, no. 9, pp. 3915-3928, Sept. 2023.

[4] W. Grabherr, W. G. B. Huder and W. Menzel, "Microstrip to waveguide transition compatible with mm-wave integrated circuits," in *IEEE Transactions on Microwave Theory and Techniques*, vol. 42, no. 9, pp. 1842-1843, Sept. 1994.

[5] D. Deslandes and K. Wu, "Integrated microstrip and rectangular waveguide in planar form," in *IEEE Microwave and Wireless Components Letters*, vol. 11, no. 2, pp. 68-70, Feb. 2001.

[6] Y. Zhao, J. Dong, F. Yin, X. Fang, and K. Xiao, "Broadband coplanar waveguide to air-filled rectangular waveguide transition," *Electronics*, vol. 11, no. 7, p. 1057, Mar. 2022.

[7] G. Gentile, B. Rejaei, V. Jovanović, L. K. Nanver, L. C. N. de Vreede and M. Spirito, "Ultra-wide band CPW to substrate integrated waveguide (SIW) transition based on a U-shaped slot antenna," *2013 European Microwave Integrated Circuit Conference*, Nuremberg, Germany, 2013, pp. 25-28.

[8] D. Lorente, M. Limbach, H. Esteban and V. Boria, "Compact ultrawideband grounded coplanar waveguide to substrate integrated waveguide tapered v-slot transition," in *IEEE Microwave and Wireless Components Letters*, vol. 30, no. 12, pp. 1137-1140, Dec. 2020.

[9] A. Patrovsky, M. Daigle and K. Wu, "Millimeter-wave wideband transition from CPW to substrate integrated waveguide on electrically thick high-permittivity substrates," *2007 European Microwave Conference*, Munich, Germany, 2007, pp. 138-141.

TABLE II. State-of-the-Art Folded Waveguide-Based Transitions

References	**Technology/Transition**	**Frequency-band**	**BW (GHz)**	**FBW (%)**	**RL (dB)**	**IL (dB)**	**Size (λ_0^3)**
[10]	PCB/GCPW-FWG	Ku	12-18	40	> 13.5	1	0.164
[11]	PCB/MS-FWG	X/Ku	7.8-13.5	53.52	> 10	> 1.25	0.035
[12]	PCB/MS-FWG	Ku	12-18	40	> 20	> 0.2	N.A.
[13]	CMOS/GCPW-FWG	G	180-220	20	> 12	> 5	0.0008
This work	Inkjet AM	X/Ku	9.08-17.54	63.61	> 10	> 1.05	0.025

MS: Microstrip. CMOS: Complementary Metal-Oxide-Semiconductor.

[10] M. D. Fernandez, J. A. Ballesteros, H. Esteban and A. Belenguer, “Folded empty substrate integrated waveguide with a robust transition to grounded coplanar waveguide in the Ku band,” in *IEEE Access*, vol. 9, pp. 76112-76118, 2021.

[11] N. Grigoropoulos, B. Sanz-Izquierdo and P. R. Young, “Substrate integrated folded waveguides (SIFW) and filters,” in *IEEE Microwave and Wireless Components Letters*, vol. 15, no. 12, pp. 829-831, Dec. 2005.

[12] A. K. Singh and S. Pal, “Development of functional broadband microstrip-to-folded SIW Ku-band transition,” in *IEEE Microwave and Wireless Technology Letters*, vol. 34, no. 1, pp. 9-12, Jan. 2024.

[13] M. Shahidzadeh Mahani and G. W. Roberts, “A mmWave folded substrate integrated waveguide in a 130-nm CMOS process,” in *IEEE Transactions on Microwave Theory and Techniques*, vol. 65, no. 8, pp. 2775-2788, Aug. 2017.

[14] B. Dogan and D. Psychogiou, “Monolithically integrated dual-channel filters using nested waveguide resonator arrays,” in *IEEE Transactions on Microwave Theory and Techniques.*

[15] C. Guo *et al*., “A 3-D printed E -plane waveguide magic-T using air-filled coax-to-waveguide transitions,” in *IEEE Transactions on Microwave Theory and Techniques*, vol. 67, no. 12, pp. 4984-4994, Dec. 2019.

[16] M. D. Nguyen, Z. Yin, R. D. Rey, F. Iacopi, and Y. Yang, “Additive manufacturing materials and processes for passive electronics in wireless communication,” *IEEE Trans. on Materials for Electron Devices*, vol. 1, pp. 97–105, 2024.

[17] J. Steele and D. Psychogiou, “Wideband broadside-coupled line baluns enabled by multimaterial additive manufacturing,” in *IEEE Transactions on Microwave Theory and Techniques*, vol. 72, no. 10, pp. 5904-5916, Oct. 2024.

[18] J. Steele and D. Psychogiou, “Self-Packaged inkjet-printed vertically integrated rf co-designed bandpass filtering baluns,” in *IEEE Transactions on Components, Packaging and Manufacturing Technology*, vol. 14, no. 11, pp. 2124-2127, Nov. 2024.

[19] B. Dogan and D. Psychogiou, “Ultra-compact inkjet-printed folded waveguide resonator-based bandpass filters,” *2025 European Microwave Conference*, Utrecht, Netherlands, 2025.

[20] M. Li, Y. Yang, Y. Zhang and F. Iacopi, “3-D printed vertically integrated composite right/left-handed transmission line and its applications to microwave circuits,” in *IEEE Transactions on Microwave Theory and Techniques*, vol. 72, no. 6, pp. 3311-3321, June 2024.